

Coherence properties of spinor condensates at finite temperatures

Krzysztof Gawryluk,¹ Mirosław Brewczyk,¹ Mariusz Gajda,² and Kazimierz Rzążewski³

¹ *Instytut Fizyki Teoretycznej, Uniwersytet w Białymstoku, ulica Lipowa 41, 15-424 Białystok, Poland*

² *Instytut Fizyki PAN, Aleja Lotników 32/46, 02-668 Warsaw, Poland*

³ *Centrum Fizyki Teoretycznej PAN, Aleja Lotników 32/46, 02-668 Warsaw, Poland*

(Dated: February 26, 2019)

We consider a spinor condensate of ⁸⁷Rb atoms in its $F = 1$ hyperfine state at finite temperatures. Putting initially all atoms in $m_F = 0$ component we find that the system evolves into the state of thermal equilibrium. This state is approached in a step-like process and when established it manifests itself in distinguishable ways. The atoms in states $m_F = +1$ and $m_F = -1$ start to rotate in opposite directions breaking the chiral symmetry and showing highly regular spin textures. Also the coherence properties of the system changes dramatically. Depending on the strength of spin-changing collisions the system first enters the stage where the $m_F = +1$ and $m_F = -1$ spinor condensate components periodically loose and recover their mutual coherence whereas their thermal counterparts get completely dephased. For stronger spin changing collisions the system enters the regime where also the strong coherence between other components is built up.

Since a ²³Na atoms Bose-Einstein condensate was created in a pure optical trap [1] it has become possible to study the spinor properties of alkali dilute quantum gases. In such (spinor) condensates the atoms can change their spins upon collisions and still remain trapped. Therefore, in spinor condensates the population of their components is allowed to change in time. This new degree of freedom distinguishes the spinor condensates from mixtures of quantum gases.

There has been recently a growing interest in such systems. Different ground-state phases (ferromagnetic or polar) have been observed experimentally in $F = 1$ condensates [2, 3, 4]. In particular, it has been shown that the ground state of rubidium condensate exhibits a ferromagnetic behavior whereas the sodium system reveals the polar phase. For a $F = 2$ manifold the set of possible ground states of spinor condensates is even richer, including the so-called cyclic phase [5]. Experiment proved that under the natural conditions a ⁸⁷Rb condensate shows a polar behavior [3]. Recently, a first $F = 3$ (⁵²Cr) condensate has been achieved [6] and many new spin phases were predicted for this system [7].

There has been also recently an interest in the dynamics of the spinor condensates, including the coherent oscillations between various components [3, 4], formation of domains [8], magnetically tuned resonances [9], and predicted theoretically the effect of breaking of chiral symmetry [10]. Some theoretical effort has been made to explore the dipolar interactions in addition to the short-range (van der Waals) interactions. In Ref. [7, 11] the coupling between the spin and orbital motion, inherently built in the dipolar interaction, is investigated and the phenomenon of the Einstein-de Haas effect is exhibited. As has been shown in Ref. [12] this effect might be observable even in a very weak dipolar systems such as rubidium condensate provided the experiment is performed under resonance condition.

In this Letter we investigate temperature properties of a spinor condensate of ⁸⁷Rb atoms in $F = 1$ hyperfine state. The influence of finite temperature on spinor evo-

lution has been studied recently experimentally [13] and theoretically although in a quasi-one-dimensional system [14]. In the second quantization notation, the Hamiltonian of the system is given by [15]

$$H = \int d^3r \left[\hat{\psi}_i^\dagger(\mathbf{r}) H_0 \hat{\psi}_i(\mathbf{r}) + \frac{c_0}{2} \hat{\psi}_j^\dagger(\mathbf{r}) \hat{\psi}_i^\dagger(\mathbf{r}) \hat{\psi}_i(\mathbf{r}) \hat{\psi}_j(\mathbf{r}) + \frac{c_2}{2} \hat{\psi}_k^\dagger(\mathbf{r}) \hat{\psi}_i^\dagger(\mathbf{r}) \mathbf{F}_{ij} \mathbf{F}_{kl} \hat{\psi}_j(\mathbf{r}) \hat{\psi}_l(\mathbf{r}) \right], \quad (1)$$

where repeated indices have to be summed over the values $m_F = +1, 0, -1$. The field operator $\hat{\psi}_i(\mathbf{r})$ annihilates an atom in the hyperfine state $|F = 1, m_F = i\rangle$ at point \mathbf{r} . The Hamiltonian consists of the kinetic energy and the trapping potential ($H_0 = -\frac{\hbar^2}{2M} \nabla^2 + V_{tr}$, where M is the mass of an atom) and two terms which describe the spin-independent and spin-dependent parts of the contact interactions, respectively. Coefficients c_0 and c_2 can be expressed with the help of the scattering lengths a_0 and a_2 which determine the collision of atoms in a channel of total spin 0 and 2. The appropriate formulas are given by $c_0 = 4\pi\hbar^2(a_0 + 2a_2)/3M$ and $c_2 = 4\pi\hbar^2(a_2 - a_0)/3M$ [15]. According to Ref. [16], $a_0 = 5.387$ nm and $a_2 = 5.313$ nm. Moreover, \mathbf{F} are the spin-1 matrices.

Within the classical fields approximation [17] one replaces the field operators $\hat{\psi}_i(\mathbf{r})$ by the classical wavefunctions $\psi_i(\mathbf{r})$. The equation of motion for these wavefunctions is written as

$$i\hbar \frac{\partial}{\partial t} \begin{pmatrix} \psi_1 \\ \psi_0 \\ \psi_{-1} \end{pmatrix} = \mathcal{H} \begin{pmatrix} \psi_1 \\ \psi_0 \\ \psi_{-1} \end{pmatrix}. \quad (2)$$

The diagonal part of \mathcal{H} is given by $\mathcal{H}_{11} = H_0 + (c_0 + c_2) |\psi_1|^2 + (c_0 + c_2) |\psi_0|^2 + (c_0 - c_2) |\psi_{-1}|^2$, $\mathcal{H}_{00} = H_0 + (c_0 + c_2) |\psi_1|^2 + c_0 |\psi_0|^2 + (c_0 + c_2) |\psi_{-1}|^2$, $\mathcal{H}_{-1-1} = H_0 + (c_0 - c_2) |\psi_1|^2 + (c_0 + c_2) |\psi_0|^2 + (c_0 + c_2) |\psi_{-1}|^2$. The off-diagonal terms describe the collisions which do not preserve the projection of spin of each atom (however, the total spin projection is conserved) and equal $\mathcal{H}_{10} = c_2 \psi_{-1}^* \psi_0$, $\mathcal{H}_{0-1} = c_2 \psi_0^* \psi_1$. Moreover, $\mathcal{H}_{1-1} = 0$.

To study the properties of a spinor condensate at finite temperatures we prepare initially an atomic sample in the $m_F = 0$ component [3] and allow the system to evolve. The Bose gas is confined in a pancake-shaped trap with the aspect ratio $\beta = \omega_z/\omega_r = 80$ and the radial frequency $\omega_r = 2\pi \times 100$ Hz. To simplify calculations, we solve numerically the Eq. (2) on a two-dimensional grid using rescaled scattering lengths (i.e., multiplied by a factor $\sqrt{\beta/2\pi}$). Obviously, spin changing collisions allow transitions to other Zeeman states ($m_F = \pm 1$) and hence the interplay between the spin dynamics and the thermalization processes can be studied. In Fig. 1a we plot the kinetic energy of each spinor component as a function of time for the initial thermal noise introduced to the $m_F = 0$ component resulting in its $\approx 20\%$ depletion. We find that after some time the kinetic energy becomes equally distributed among spinor components (see Fig. 1), suggesting the system reached an equilibrium. The time needed for that depends on the initial amount of the thermal noise (the higher thermal energy the longer relaxation time). However, approaching this equilibrium is rather a step-like process not a uniform one. This is because the atomic cloud becomes fragmented and the overlap of different spin components changes significantly in time (Fig. 1a, green curve). The steps in Fig. 1a seem to correspond to the maximal overlap.

Spin changing collisions between atoms in $m_F = 0$ state produce equally atoms in states $m_F = \pm 1$. Initially, both condensed and thermal atoms go to the $m_F = \pm 1$ components and back (see Fig. 1b). This behavior changes after the equilibrium is established, i.e., after 0.6s. From now on, the fraction of thermal atoms in each component becomes 1/3 (Fig. 1b, main frame). Since the total number of thermal atoms is also constant the system reaches the thermal equilibrium meaning all spin components in the thermal cloud are equally populated (already observed experimentally [13]). At the same time a non-trivial spin dynamics for condensed atoms is observed (Fig. 1b, inset). Thus, the spinor condensate decouples from the thermal cloud. Also, since the condensed atoms do not populate equally spinor components (as the thermal atoms do) it means that the single mode approximation is inappropriate at finite temperatures.

To discuss the coherence properties of spinor condensates it is necessary to have in mind the stability diagram for such a system. This diagram is formed as a result of the Bogoliubov-de Gennes analysis of Eq. (2) in two-dimensional space and is considered with respect to the parameters (c_2, c_0) . More precisely, the stability of $m_F = 0$ component against the excitations in $m_F = \pm 1$ states is investigated with particular emphasis on modes of types $\propto e^{im\phi}$, where $m = \pm 1, 0$ (see Ref. [10]). This analysis proves the existence of the regions where all $m = \pm 1, 0$ modes are stable, only modes $m = \pm 1$ are unstable, and all $m = \pm 1, 0$ modes are unstable. The coherence properties strongly depend on which region the systems parameters belong to. For example, if modes $m = \pm 1$ get unstable the superposition

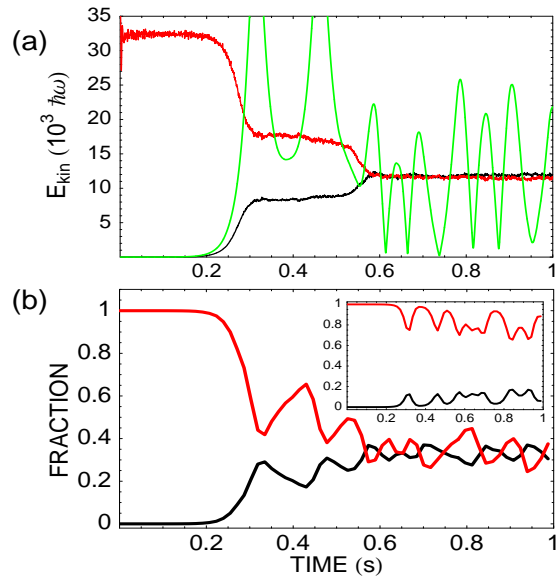


FIG. 1: (color online). (a) Kinetic energy of spinor components as a function of time for $m_F = 0$ (red color) and $m_F = \pm 1$ (black color) Zeeman states. The green line is the overlap between the $+1$ and -1 components defined by the scalar product $|\langle \psi_{+1}, \psi_{-1} \rangle|$. (b) Fraction of total thermal (main frame) and total condensed (inset) atoms in each spinor component (red for 0 and black for ± 1 states).

of $\propto e^{i\phi}$ and $\propto e^{-i\phi}$ states is excited in $m_F = 1$ (as well as in $m_F = -1$) component. Assuming both modes equally contribute to this superposition one should expect the fragmented (and consisted of two parts) densities in $m_F = \pm 1$ components. Examples are given in Fig. 2. This fragmentation and circulation of atomic clouds are responsible for the coherence properties discussed below. Note also that the thermal atoms cause the granularity of densities since decreasing the level of initial thermal noise leads to very smooth densities.

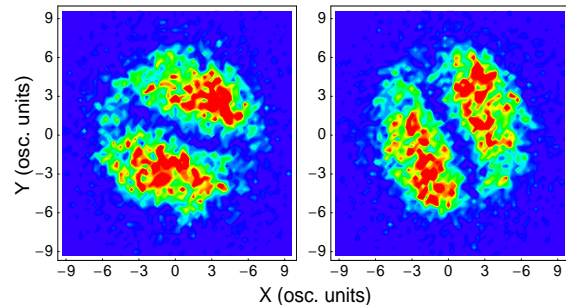


FIG. 2: (color online). Density of $+1$ (left frame) and -1 (right frame) components for $c_2 = -1.0 \times 10^{-3}$, $c_0 = 0.22$, and $E_{\text{kin}}(0) = 9 \times 10^3$ osc. units at 0.8 s.

To investigate in detail the coherence properties of spinor condensates we calculate the one-particle density

matrix by averaging the product $\Psi^*(\mathbf{r}, t)\Psi(\mathbf{r}', t)$ (with the spinor classical field $\Psi(\mathbf{r}, t)$ being the solution of Eq. (2)) over the finite volume [17]. Next, this matrix is diagonalized and an eigenvector corresponding to the dominant eigenvalue represents the spinor condensate wave function. Let us denote it by $\varphi_0(\mathbf{r}, t)$. Then the thermal component of the spinor classical field can be defined as $\psi^T = \Psi - (\varphi_0, \Psi)\varphi_0$ (here, the vector φ_0 is normalized to unity). Thermal part of the classical field lives in a space orthogonal to the condensate wave function. Now we introduce the spin density matrices for the condensate and the thermal part as below

$$\begin{aligned}\rho_{ij}^0 &= \int \varphi_{0i}^*(\mathbf{r}) \varphi_{0j}(\mathbf{r}) d^3r \\ \rho_{ij}^T &= \int \psi_i^{T*}(\mathbf{r}) \psi_j^T(\mathbf{r}) d^3r.\end{aligned}\quad (3)$$

These matrices tell us about the inherent coherence of the spinor condensate and the thermal cloud. It is convenient to consider the normalized spin density matrices $\tilde{\rho}_{ij} = \rho_{ij} / \sqrt{\rho_{ii}\rho_{jj}}$. The diagonal elements of such matrices are equal to one and their off-diagonal elements determine the degree of coherence between various components of spinor condensate or the thermal cloud. When the off-diagonal element takes the value of the order of one (note that the maximal value of $|\tilde{\rho}_{ij}|$ equals 1) the coherence is strong whereas opposite means that the components are completely dephased.

Coherence properties of ^{87}Rb spinor condensate are displayed in Fig. 3, where we show time dependence of spin density matrix elements corresponding to different regimes of parameters according to the stability analysis. When the coupling constant c_2 is negative (ferromagnetic phase) and large enough to develop the rotational instability (i.e., when modes $m = \pm 1$ become unstable) the strong coherence between the $+1$ and -1 spinor condensate components builds up (upper frame). This coherence is maximal while the system is approaching the thermal equilibrium and remains strong afterwards, however, in a way that it is periodically lost and restored. Surprisingly, even thermal cloud in components $+1$ and -1 is fully coherent during the way of the system to its equilibrium but later on (after 0.6 s) the thermal components get completely dephased. In this particular regime of parameters (c_2, c_0) we observe only a development of coherence between $+1$ and -1 components. This can be understood by comparing the overlaps $|(\psi_{+1}, \psi_{-1})|$ and $|(\psi_{+1}, \psi_0)|$ during the evolution – the latter one turns out to be negligible.

However, the situation changes when the strength of spin-changing collisions c_2 becomes large enough (and still negative) to develop an instability leading to significant population of $m_F = \pm 1$ Zeeman states with non-rotating atoms (i.e., when the mode $m = 0$ becomes unstable). In the case of Fig. 3b the system reaches its equilibrium already after 0.2 s and then the overlap $|(\psi_{+1}, \psi_0)|$ gets even larger than the $|(\psi_{+1}, \psi_{-1})|$ one and it results in a development of coherence between $+1$ and

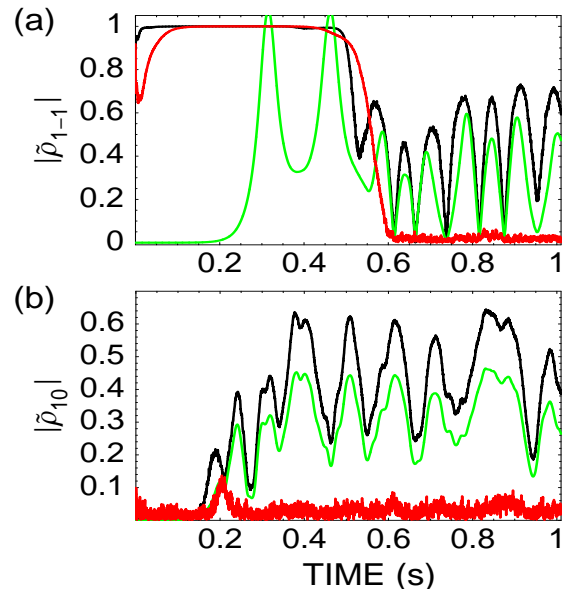


FIG. 3: (color online). Spin density off-diagonal elements for (a) $(+1, -1)$ components ($c_2 = -1.0 \times 10^{-3}$, $c_0 = 0.22$, and $E_{kin}(0) = 32 \times 10^3$) and (b) $(+1, 0)$ components ($c_2 = -2.29 \times 10^{-3}$, $c_0 = 0.50$, and $E_{kin}(0) = 22 \times 10^3$) for the condensate (black line) and the thermal cloud (red line) as a function of time. The overlaps $|(\psi_{+1}, \psi_{-1})|$ and $|(\psi_{+1}, \psi_0)|$ are plotted in green in (a) and (b), respectively.

0 components. The same is true for the pair of -1 and 0 states. Therefore, in this range of (c_2, c_0) parameters all components of spinor condensates remain mutually coherent. Note that the thermal parts in $+1$ and 0 states are always dephased.

Both frames show also the overlaps: $|(\psi_{+1}, \psi_{-1})|$ in (a) and $|(\psi_{+1}, \psi_0)|$ in (b) case in green color. In the equilibrium the spin density off-diagonal elements follow the corresponding overlaps. It clearly indicates that the coherence is built as a result of many atomic collisions. They allow to establish the relative phase of the components. In case (a) in the equilibrium the phase of the off-diagonal element $\tilde{\rho}_{1,-1}$ becomes fixed within the intervals which correspond to the maximal overlap but changes going from one maximum to the other. On the other hand, in (b) the phase of $\tilde{\rho}_{1,0}$ gets constant just after the system reaches the thermal equilibrium (i.e., after 0.2 s).

Another peculiar feature of spinor condensates revealed after the system reaches its equilibrium is breaking of the chiral symmetry (at zero temperature this phenomenon was already reported in [10]). Since the modes $m = \pm 1$ get unstable the atoms in components $+1$ and -1 start to rotate in opposite directions (the total orbital angular momentum projection of colliding atoms is preserved by the contact interactions) on the onset of the equilibrium. No spontaneous rotation is observed when the system is approaching the equilibrium state. Fig. 4a (curves black, red, and green) shows the typical behav-

ior of the angular momentum of all components when $c_0/c_2 = -216.4$ (this is the natural ratio for $F = 1$ ^{87}Rb atoms). In components $+1$ and -1 the atoms rotate alternatively clockwise and counterclockwise. This property changes when c_0/c_2 differs strongly from -216.4 . In this case components rotate only in one direction permanently breaking the chiral symmetry (blue curve in Fig. 4a). Note, that unlike in [10] this permanent rotation is obtained here in the conservative, hamiltonian dynamics.

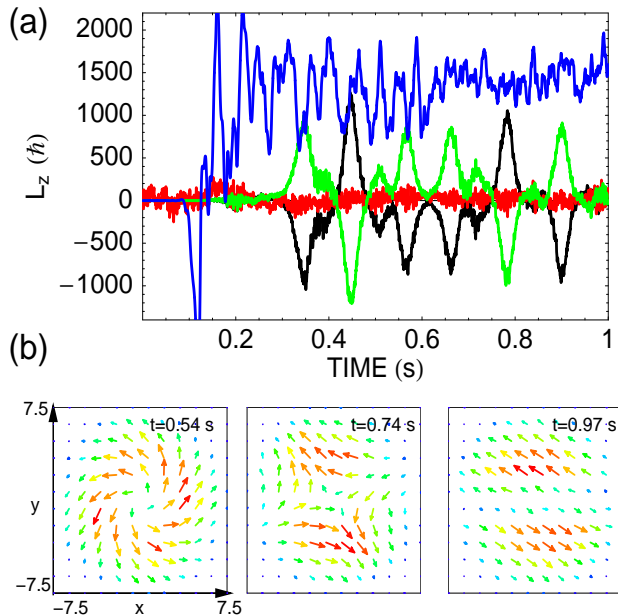


FIG. 4: (color online). (a) Angular momentum of components $m_F = +1$ (black curve), $m_F = 0$ (red curve), and $m_F = -1$ (green curve) as a function of time for parameters $c_2 = -1.0 \times 10^{-3}$, $c_0 = 0.22$, and $E_{kin}(0) = 9 \times 10^3$. Blue curve shows the angular momentum of $m_F = +1$ state in the case when $c_0/c_2 \neq -216.4$ ($c_2 = -4.06 \times 10^{-3}$, $c_0 = 0.25$). (b) Spin textures at particular instants of time for parameters (c_2, c_0) as in the first case of part (a). The length of the vector (as well as the color) represents the quantity $(\langle F_x \rangle^2 + \langle F_y \rangle^2)^{1/2}$ and the size of each frame is 15×15 oscillatory units.

It turns out that the periods the atoms in $m_F = +1$ or $m_F = -1$ states rotate in one direction (black and green lines in Fig. 4a) coincide with those when the off-diagonal

spin density matrix element $|\hat{\rho}_{1-1}|$ takes large values, i.e., when the mutual coherence between $m_F = +1$ and $m_F = -1$ components is built up. In these time intervals the system develops also highly regular spin textures. Examples are given in lower panel in Fig. 4 where we plot the vector field composed of the average values of the total spin at particular instants of time. The first (from the left) frame shows the spiral galaxy-like pattern which persists within the interval $(0.52 - 0.62)$ s. Later on a quadrupole-like texture is developed and lasts from 0.74 s to 0.81 s (the second frame). The third plot shows domain-like pattern. On the other hand, for the case when atoms rotate in one direction (blue curve) the system exhibits all the time the same structure which for the parameters considered is a spiral galaxy-like one.

In conclusion, we have shown that the initially randomly disturbed spinor condensate enters the equilibrium state in a step-like process. Counter intuitively, the dynamics of the system becomes rich when it gets into the equilibrium. The atoms in components $m_F = +1$ and $m_F = -1$ spontaneously rotate in opposite directions and the magnetization shows the regular textures. Moreover, the system exhibits coherence properties dependent on the strength of the spin-changing collisions. When such collisions are not strong enough but still allowing the transition to other Zeeman states only spinor components $m_F = \pm 1$ develop the mutual coherence. We observe that this coherence is periodically lost and restored. Simultaneously, the corresponding thermal parts get completely dephased. For larger values of coupling constants c_2 the system enters a new regime where the coherence between components $m_F = 0$ and $m_F = \pm 1$ is developed and becomes as strong as for $m_F = +1$ and $m_F = -1$ states.

Acknowledgments

M.B., and M.G. acknowledge support by the Polish KBN Grant No. 1 P03B 051 30. K.G. thanks the Polish Ministry of Scientific Research Grant Quantum Information and Quantum Engineering No. PBZ-MIN-008/P03. This paper (K.R.) was funded by Polish Government research funds for 2006-2009.

-
- [1] D.M. Stamper-Kurn *et al.*, Phys. Rev. Lett. **80**, 2027 (1998).
 - [2] J. Stenger *et al.*, Nature **396**, 345 (1998).
 - [3] H. Schmaljohann *et al.*, Phys. Rev. Lett. **92**, 040402 (2004).
 - [4] M.-S. Chang *et al.*, Phys. Rev. Lett. **92**, 140403 (2004).
 - [5] C.V. Ciobanu, S.-K. Yip, and T.-L. Ho, Phys. Rev. A **61**, 033607 (2000); M. Koashi and M. Ueda Phys. Rev. Lett. **84**, 1066 (2000).
 - [6] A. Griesmaier *et al.*, Phys. Rev. Lett. **94**, 160401 (2005).
 - [7] L. Santos and T. Pfau, Phys. Rev. Lett. **96**, 190404 (2006).
 - [8] L.E. Sadler *et al.*, cond-mat/0605351.
 - [9] J. Kronjäger *et al.*, cond-mat/0606046.
 - [10] H. Saito, Y. Kawaguchi, and M. Ueda, Phys. Rev. Lett. **96**, 065302 (2006).
 - [11] Y. Kawaguchi, H. Saito, and M. Ueda, Phys. Rev. Lett. **96**, 080405 (2006).
 - [12] K. Gawryluk *et al.*, cond-mat/0609061.
 - [13] M. Erhard *et al.*, Phys. Rev. A **70**, 031602(R) (2004); J.

- Kronjäger *et al.*, Phys. Rev. A **72**, 063619 (2005).
- [14] J. Mur-Petit *et al.*, Phys. Rev. A **73**, 013629 (2006).
- [15] T.-L. Ho, Phys. Rev. Lett. **81**, 742 (1998); T. Ohmi and K. Machida, J. Phys. Soc. Jap. **67**, 1822 (1998).
- [16] E.G.M. van Kempen *et al.*, Phys. Rev. Lett. **88**, 093201 (2002).
- [17] For a review of classical fields approximation see M. Brewczyk, M. Gajda, and K. Rzążewski, J. Phys. B **40**, R1 (2007).